

MedChemComm

Accepted Manuscript



This article can be cited before page numbers have been issued, to do this please use: R. Duroux, A. Ciancetta, P. Mannes, J. Yu, S. Boyapati, E. Gizewski, S. Yous, F. Ciruela, J. Auchampach, Z. Gao and K. Jacobson, *Med. Chem. Commun.*, 2017, DOI: 10.1039/C7MD00247E.



This is an Accepted Manuscript, which has been through the Royal Society of Chemistry peer review process and has been accepted for publication.

Accepted Manuscripts are published online shortly after acceptance, before technical editing, formatting and proof reading. Using this free service, authors can make their results available to the community, in citable form, before we publish the edited article. We will replace this Accepted Manuscript with the edited and formatted Advance Article as soon as it is available.

You can find more information about Accepted Manuscripts in the [author guidelines](#).

Please note that technical editing may introduce minor changes to the text and/or graphics, which may alter content. The journal's standard [Terms & Conditions](#) and the ethical guidelines, outlined in our [author and reviewer resource centre](#), still apply. In no event shall the Royal Society of Chemistry be held responsible for any errors or omissions in this Accepted Manuscript or any consequences arising from the use of any information it contains.

Bitopic Fluorescent Antagonists of the A_{2A} Adenosine Receptor Based on Pyrazolo[4,3-*e*][1,2,4]triazolo[1,5-*c*]pyrimidin-5-amine Functionalized Congeners

Romain Duroux,^{a,b,f} Antonella Ciancetta,^{a,f} Philip Mannes,^a Jinha Yu,^a Shireesha Boyapati,^{a,c} Elizabeth Gizewski,^d Said Yous,^b Francisco Ciruela,^e John A. Auchampach,^d Zhan-Guo Gao,^a
and Kenneth A. Jacobson^{a*}

^a Molecular Recognition Section, Laboratory of Bioorganic Chemistry, National Institute of Diabetes and Digestive and Kidney Diseases, National Institutes of Health, Bethesda, MD 20892.

^b Univ. Lille, Inserm, CHU Lille, UMR-S 1172 - JPArc - Centre de Recherche Jean-Pierre AUBERT Neurosciences et Cancer, F-59000 Lille, France.

^c Department of Pharmaceutical Chemistry, Telangana University, Nizamabad, Telangana, India 503322.

^d Department of Pharmacology, Medical College of Wisconsin, 8701 Watertown Plank Road, Milwaukee, Wisconsin 53226 USA.

^e Unitat de Farmacologia, Departament Patologia i Terapeutica Experimental, Facultat de Medicina, IDIBELL, Universitat de Barcelona, 08907 L'Hospitalet de Llobregat, Spain.

^f Contributed equally.

Corresponding author: Dr. K.A. Jacobson, Chief, Molecular Recognition Section, Bldg. 8A, Rm. B1A-19, NIH, NIDDK, LBC, Bethesda, MD 20892-0810. *Tel:* 301-496-9024. *Fax:* 301-480-8422; *Email:* kennethj@niddk.nih.gov

ABBREVIATIONS: AN, acetonitrile; AR, adenosine receptor; BODIPY, 4,4-difluoro-4-bora-3a,4a-diaza-s-indacene; CNS, central nervous system; DMF, *N,N*-dimethylformamide; EDC, *N*-(3-dimethylaminopropyl)-*N'*-ethylcarbodiimide; HEK, human embryonic kidney; IE, interaction energy; NECA, 5'-*N*-ethylcarboxamidoadenosine; PD, Parkinson's disease; TBAP, tetrabutylammonium dihydrogen phosphate; THF, tetrahydrofuran; TLC, thin layer chromatography; TM, transmembrane domain.

Abstract

A pyrazolo[4,3-*e*][1,2,4]triazolo[1,5-*c*]pyrimidin-5-amine antagonist of the A_{2A} adenosine receptor (AR) was functionalized as amine congeners, fluorescent conjugates and a sulfonate, and A_{2A}AR binding modes were predicted computationally. The optimal *n*-butyl spacer was incorporated into the following A_{2A}AR-selective (K_i, nM) conjugates: BODIPY630/650 derivative **11** (MRS7396, 24.6) and Alexafluor488 derivative **12** (MRS7416, 30.3). Flow cytometry of **12** in hA_{2A}AR-expressing HEK-293 cells displayed saturable binding (low nonspecific) and inhibition by known A_{2A}AR antagonists. Water-soluble sulfonate **13** was a highly potent (K_i = 6.2 nM) and selective A_{2A}AR antagonist based on binding and functional assays. Docking and molecular dynamics simulations predicted the regions of interaction of the distal portions of these chain-extended ligands with the A_{2A}AR. The BODIPY630/650 fluorophore of **11** was buried in a hydrophobic interhelical (TM1/TM7) region, while AlexFluor488 of **12** associated with the hydrophilic extracellular loops. In conclusion, we have identified novel high affinity antagonist probes for A_{2A}AR drug discovery and characterization.

Keywords: adenosine antagonist; SCH442416; G protein-coupled receptor; fluorescence; radioligand binding.

Introduction

The development of selective agonists and antagonists of the four subtypes of adenosine receptors (ARs) has been extensively explored.¹⁻³ Antagonists of the G_s protein-coupled A_{2A}AR are sought as agents for treating neurodegenerative conditions such as Parkinson's disease (PD) and Alzheimer's disease (AD), and for coadministration with cancer immunotherapy.⁴⁻⁷ Caffeine, the most consumed psychostimulant in the world, acts as a nonselective AR antagonist and readily enters the brain to antagonize the A_{2A}AR at doses generally consumed. Epidemiological evidence showing a lower occurrence of AD and PD with modest caffeine intake points to the possibility that caffeine consumption is neuroprotective. Indeed, A_{2A}AR antagonists can exert a neuroprotective effect against excitotoxicity in animal models; one mechanism appears to be enhancing the activity of an A₁AR, which forms a heterodimer with A_{2A}AR, to inhibit glutamate release.⁸ A_{2A}AR antagonists also control microglia-mediated neuroinflammation.⁹ Therefore, it is possible that A_{2A}AR antagonists may also delay neurodegenerative disease progression. In the striatum, A_{2A}AR antagonists act to boost dopaminergic signaling, and thus provide symptomatic relief to reduce the motor deficits in PD without inducing dyskinesia. Certain selective A_{2A}AR antagonists, e.g. **1-4** (Chart 1), have been shown to enter the brain in sufficient levels for imaging and efficacy in PD models.¹⁰⁻¹² A caffeine-like 1,3,7-trialkylxanthine, istradefylline **1** is approved in Japan for treating PD, and its safety and efficacy in reducing in off-time in levodopa-treated patients were established in a 52-week trial.¹⁰ A tricyclic pyrazolo-triazolopyrimidine derivative **4**, which binds potently and selectively to the A_{2A}AR, was in clinical trials for PD.¹²

In the periphery, elevated adenosine levels present in the microenvironment of tumors lead to a suppressed immune response, to shift the T cell response away from an aggressive state capable of attacking tumors.⁶ Increasing evidence supports the use of AR antagonists in cancer treatment, either

with selectivity for A_{2A}AR alone or with dual selectivity for A_{2A}AR and A_{2B}AR. Cytokine production in CD8⁺ chimeric antigen receptor (CAR) T cells was increased, and both CD8⁺ and CD4⁺ CAR T cells were activated upon blocking the A_{2A}AR.⁷ Thus, there is great interest in the discovery of novel A_{2A}AR antagonists to act either centrally or peripherally, and new tools for ligand discovery are needed.

Various fluorescent probes have been developed over the past few years for characterizing ARs,¹³⁻¹⁵ and their use in fluorescence polarization (FP), fluorescence resonance energy transfer (FRET) and flow cytometry (FCM) has proven feasible. Moreover, these ligands can provide a better understanding of receptor location, function and regulation. Most of the reported fluorescent A_{2A}AR antagonists used 5-amino-7-(3-(4-methoxy)phenylpropyl)-2-(2-furyl)pyrazolo[4,3-e]-1,2,4-triazolo[1,5-c]pyrimidine (SCH442416, **3**) as the pharmacophore due to a *p*-methoxyphenylpropyl side chain moiety of the antagonist, which served as the site for attachment of functionalized chains through an ether linkage.

Much of the ligand development for ARs now benefits from a detailed structural knowledge of the human (h)A_{2A}AR.¹⁶⁻²⁰ More than two dozen high-resolution X-ray crystallographic A_{2A}AR structures with bound agonist or antagonist have been determined and used for the in silico screening of chemical libraries. A_{2A}AR complexes with antagonist 4-[2-[7-amino-2-(2-furyl)-1,2,4-triazolo[1,5-a][1,3,5]triazin-5-yl-amino]ethylphenol (ZM241385, **2**) show that the heterocyclic pharmacophore binds to residues in the orthosteric binding pocket that also coordinate the adenine moiety of AR agonists.^{16,17} Although there is no X-ray structure of a **3**-A_{2A}AR complex, we used the **2**-A_{2A}AR structure as structural template for molecular modeling. The hypothetical docking pose of **3** and its AlexaFluor488 derivative **5** established most of the conserved interactions in the orthosteric binding site.^{13,14} The

modeling also predicted stabilizing interactions of the tethered fluorophore with specific charged and H-bonding residues of the second extracellular loop (EL2).

Conjugate **5** was not optimal for fluorescent binding due to its moderate hA_{2A}AR affinity ($K_i = 111$ nM).¹³ Also, its green light emission presents difficulties in fluorescence microscopy due to cell autofluorescence. Thus, there remains a need for A_{2A}AR antagonist fluorescent probes of higher affinity and compatibility with microscopy. A BODIPY650/655 conjugate containing a secondary amine in the linking chain was reported to have a K_i value of 15 nM at the A_{2A}AR, but its utility was not established.¹³ With this aim, we explored further the SAR of the distal region of this chemical series by varying the chain length of the spacer group and the terminal fluorophore in order to enhance affinity, selectivity and photophysical properties.

6

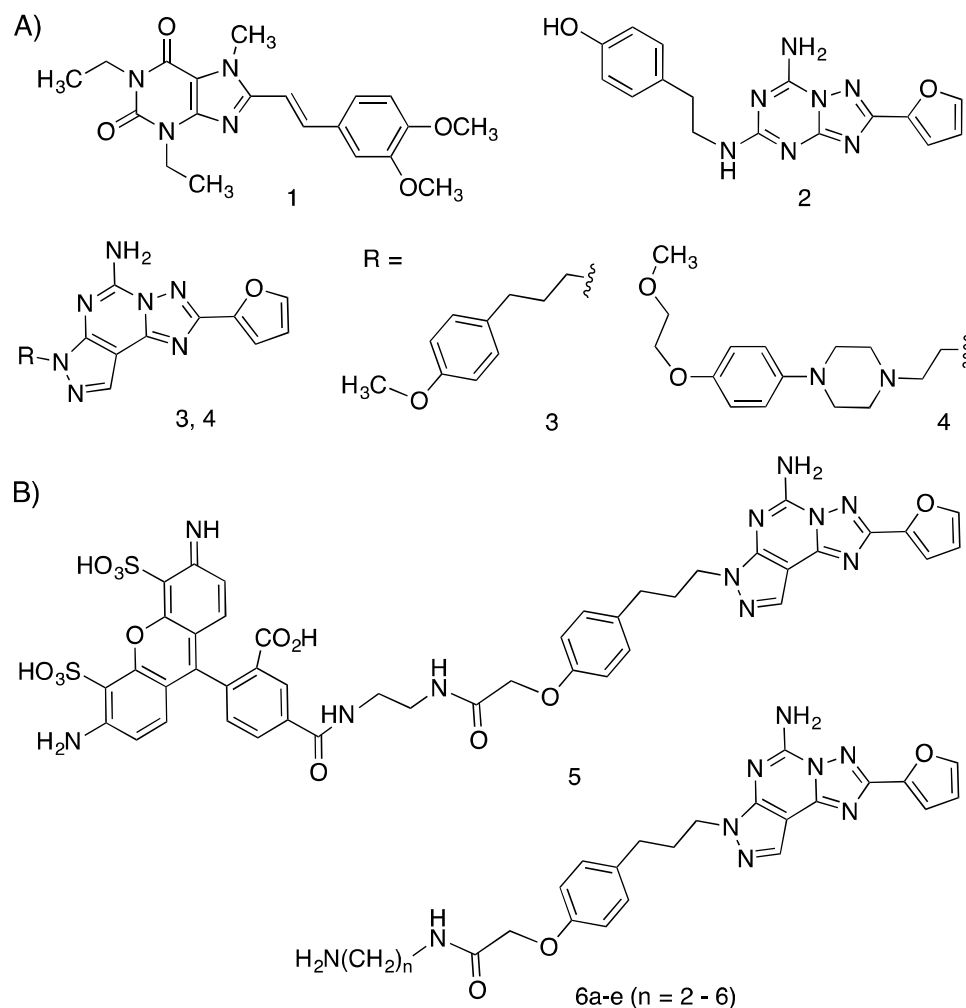


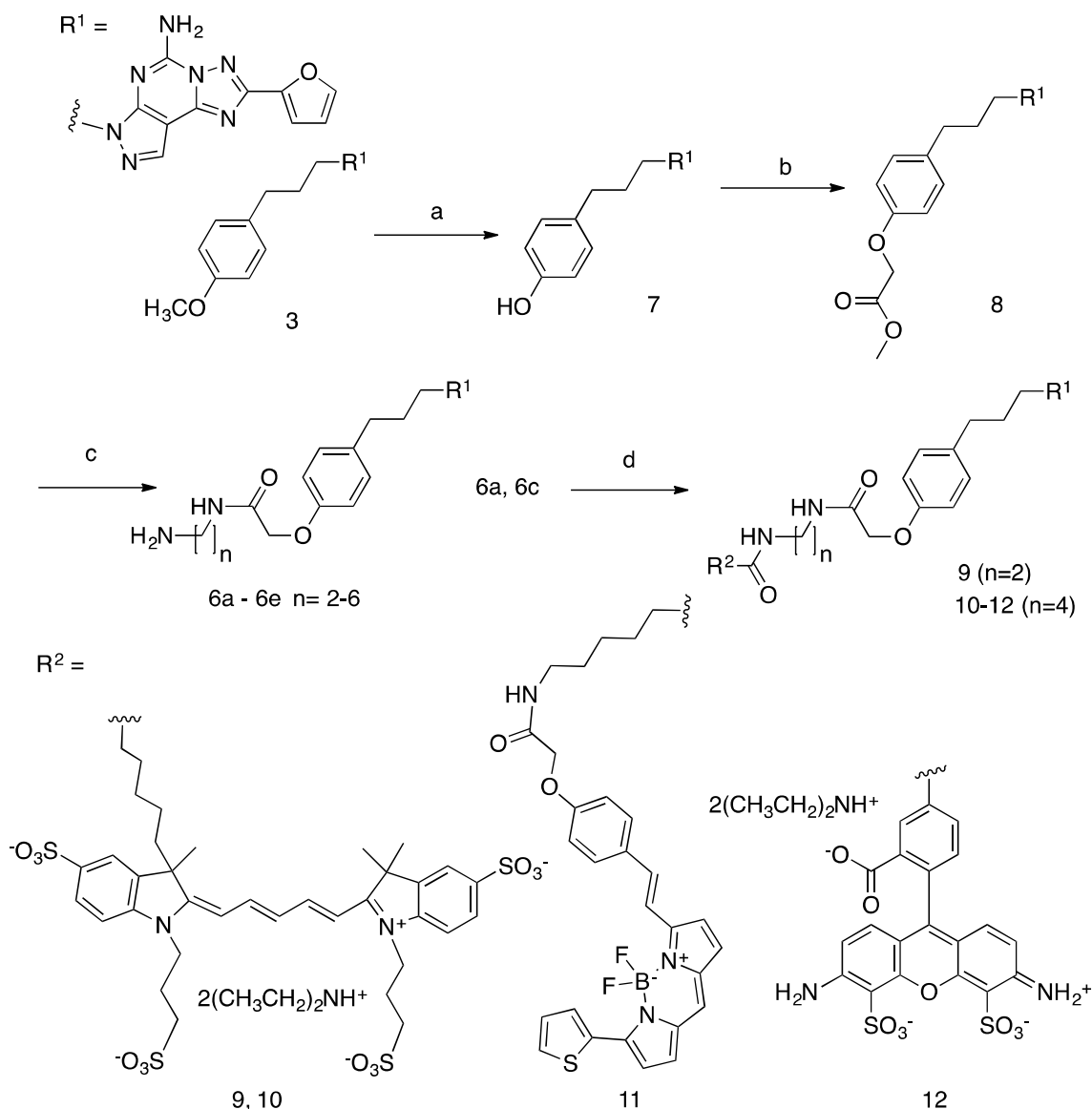
Chart 1. Structures of selective $A_{2A}AR$ antagonists and the target series: (A) Widely used pharmacological probes and clinical candidates (**1-4**); (B) A reported fluorescent probe **5** derived from **3** and functionalized amine congeners of varied chain length **6** explored in this study.

Results and Discussion

We initially prepared a series of primary amine congeners of an $A_{2A}AR$ antagonist **3** by extending the *p*-methoxyphenylpropyl chain, which is predicted to lie outside the orthosteric binding site of the pharmacophore and be able to reach accessory sites.¹³ The congener **6a** (n = 2) was reported earlier,¹³

and we hypothesized that extension of the alkyl spacer could enhance affinity or selectivity at this receptor, perhaps by establishing H-bond or electrostatic interactions with polar residues in the EL region of the A_{2A}AR. The synthesis of the pyrazolo[4,3-*e*][1,2,4]triazolo[1,5-*c*]pyrimidin-5-amine derivatives is shown in Scheme 1.

The synthesis of fluorescent ligands **9-12** was accomplished in 4 steps from commercially available **3**. The latter was demethylated to **7** by the action of BBr₃ and then treated with an excess of methyl-2-bromoacetate (12 eq.) and Cs₂CO₃ as base to provide ester **8** in 90% yield. Other methods, such as using NaH as base with 1 eq. of methyl 2-bromoacetate in DMF, were attempted but led to the formation of di and tri-alkylated compounds. Amide synthesis was then performed by treatment of ester **8** with a series of alkyl diamines to give the amine congeners **6a-e**. Two of these amines, **6a** (n = 2) and **6c** (n = 4), were reacted with activated fluorophore moieties in DMF in the presence of Et₃N to afford, after semi-preparative HPLC, compounds **9-12** in good yield (40-60%): cyanine 5 red fluorescent AlexaFluor647 (n=2, **9**; n=4, **10**), and red fluorescent BODIPY630/650 (n = 4, **11**) and green fluorescent AlexaFluor488 (n = 4, **12**). Both fluorophores are commonly incorporated into ligand tools for chemical biology.²¹



Scheme 1. Synthesis of $A_{2A}AR$ antagonist functionalized congeners **6** and their fluorescent derivatives **9-12**. (a) BBr_3 , CH_2Cl_2 , rt, 4h; (b) methyl 2-bromoacetate, CS_2CO_3 , MeOH, 40 °C, overnight; (c) diaminoalkane, MeOH (9:1 v/v), rt, overnight; (d) activated fluorophore (AlexaFluor647 *N*-hydroxysuccinimidyl ester for **9** and **10**, BODIPY 630/650 *N*-hydroxysuccinimidyl ester for **11**, AlexaFluor488 carboxylic acid, 2,3,5,6-tetrafluorophenyl ester for **12**), Et_3N , DMF, rt, overnight.

The affinity of the amine congeners and other antagonists was measured using standard radioligand binding assays at hA₁, A_{2A} and A₃ARs (Table 1).^{1,13,14,22} Membranes of human embryonic kidney (HEK)293 cells expressing the AR of interest were used in the assay. Primary amine congeners **6a** - **6d** containing spacers of 2 – 5 methylenes were similar in hA_{2A}AR affinity (K_i 6 - 9 nM), but the butylamino congener **6c** displayed the highest A_{2A}AR selectivity in the series. The affinity of this compound at hA₃AR was determined to be 6.0 μM, with only slightly higher hA₁AR affinity. Homologation to 6 methylenes in compound **6e** lowered A_{2A}AR affinity. Among the fluorescent conjugates of butylamino congener **6c**, i.e. **10**, **11**, and **12**, the highest A_{2A}AR affinity and selectivity were observed with the BODIPY630/650 fluorophore **11** and AlexaFluor488 **12** (Figure 1). Thus, fluorescent **11** and **12** were only 4-fold weaker in A_{2A}AR affinity with respect to parent amino derivative **6c**. Interestingly, AlexaFluor488 conjugate **12** was at least as potent in A_{2A}AR affinity as its shorter homologue **5**. No dependence of affinity on chain length was evident when comparing AlexaFluor647 conjugates **9** and **10**. Affinity at the mouse (m) ARs was also measured for selected compounds by methods described,²² and **11** was particularly potent and selective at the mA_{2A}AR (K_i = 2.1 nM), in contrast to **12** (K_i 585 nM).

We performed a molecular modeling analysis to identify possible binding modes of fluorescent conjugates **11** and **12** using the high resolution 2-A_{2A}AR X-ray structure (PDB ID: 4EIY).¹⁷ We first docked reference compound **3** at the hA_{2A}AR by retaining several water molecules observed in the X-ray structure as described (Supporting Information). In the corresponding docking pose (Figure 2A), the pyrazolotriazolopyrimidine core of **3** docked in the orthosteric binding site similarly to the triazolopyrimidine core of **2**, with a π-π stacking interaction of the aromatic core with F168 (EL2), and a H-bonding network with N253 (6.55, using standard GPCR notation²³) and E169 (EL2). The methoxy-

phenyl substituent of **2** pointed toward the extracellular (EC) side of the receptor and interacted with the side chain of Glu169 (EL2) through a water molecule. The binding mode of **3** described above was validated using 30 ns of molecular dynamics (MD) simulation. During the simulation (Video S1, replica analysis reported in Table S1), the methoxy-phenyl moiety folded toward transmembrane domain 2 (TM2) and established a π - π stacking interaction with Y271 (7.36), while the aromatic core maintained the H-bond network observed in the initial docking pose. Notably, the most energetically favored ligand-protein complex featured the same interaction pattern described above (Figure S1).

The potent fluorescent conjugate **11** was then docked in the A_{2A}AR structure (Figure 2B) with the same water molecules retained as in the **3**-A_{2A}AR complex.¹⁷ The pyrazolotriazolopyrimidine core established the same interactions observed for **3** in the orthosteric binding site. The fluorophore linker pointed toward the EC side and folded back toward the TM bundles by directing the fluorophore group to an aromatic pocket at the interface between TM1 and TM7 (transparent surface in Figure 2B). To explore other orientations of the linker at the receptor's EC side, we docked compound **6c**, the amino precursor of **11**, at the hA_{2A}AR. To sample all the possible H-bond acceptor/donor partners on the EC side of the receptor, we removed water molecules interacting with E169 during the docking. We then clustered the binding modes obtained according to the linker orientation. This selection resulted in two alternative binding modes (Figure S2) that were subsequently subjected to MD validation (30 ns of simulation run in triplicate for each binding mode, see Table S1). In the most energetically favored docking mode (hereby referred as "BM1", orange carbon sticks in Figure S2, docking score = -12.077 kcal/mol), the tail was oriented toward TM4 and TM5 with the amide moiety establishing a H-bond with the side chain of E169, while the terminal amine group H-bonded with the backbone of E169 (EL2) and the side chain of K150 (EL2). This latter H-bond was expected to be unstable in a dynamic environment due to

competition in the formation of a salt-bridge between K150 and D170 (EL2). In the alternative binding mode (BM2, green carbon sticks in Figure S2, docking score = -10.994 kcal/mol), the tail was oriented toward TM1 and TM2 and did not establish additional interactions. MD trajectory analysis revealed that BM1 achieved ligand-protein complexes that were more energetically favored (data not shown). Figure S3 depicts the two **11**-A_{2A}AR complexes with the most favorable ligand-protein interaction energy (IE, values differed by less than 2 kcal/mol and were considered equivalent) obtained for BM1 that feature different orientations of the tail. We therefore searched for hydrophobic and aromatic regions in proximity of the terminal amine moiety to investigate the compatibility of these orientations with the fluorophore insertion. Specifically, we searched for receptor regions rich in hydrophobic and aromatic residues at 5, 13, and 14 Å from the nitrogen atom of the terminal alkylamino group of **6c** (Figure S3B). The choice of distances reflected the analysis of the N-group distance to aromatic rings in both the docked and the energy minimized three-dimensional structures of **11** (Figure S3A). Of the two possible orientations of **11**, only one displayed hydrophobic and aromatic residues at distances compatible with the insertion of the aromatic fluorophore. Notably, the aromatic/hydrophobic region is located at the interface between TM1 and TM7 (Figure S3C), thus suggesting the same orientation of the ligand as resulted by the docking analysis. Nonetheless, we cannot exclude that **11** might explore different regions on the receptor's EC side.

The fluorescent conjugate **12** (considered as the species carrying a -2 net charge) was docked in the A_{2A}AR structure by following the same procedure described for compound **11** (Supporting Information). The docking output suggested two equally plausible orientations of the fluorophore (Figure 2C and D). In one docking pose (BM1, cyan carbon sticks in Figure 2C, docking score = -11.490 kcal/mol), the fluorophore group was projected toward EL3. In the alternative binding mode (BM2, purple carbon

sticks, docking score = -11.279 kcal/mol), the fluorophore group interacted with residues in EL2 and EL3. The interaction pattern of the core was the same as for other members of this chemical series: H-bonds with N253 and E169 (EL2); π - π stacking with H252 (6.52), F168 (EL2), and Y271 (7.36). In the MD simulation starting from BM1 (30 ns run in triplicate, see Table S1) the fluorophore group and the linker fluctuated on the EC surface of the receptor without engaging in specific interactions except for a H-bond involving the fluorophore carboxylate moiety (data not shown). On the other hand, the simulations starting from BM2 (30 ns, replica analysis in Table S1) achieved more energetically favored ligand-protein complexes. The simulations returned the ligand-protein complex characterized by the lowest IE value for all trajectories and converged in a unique binding mode (Figure S4) featuring the fluorophore group stacked between EL2 and EL3. In such a conformation, the ligand established a tight network of H-bonds and salt-bridges between charged residues in EL2 and EL3 and polar/charged counterparts in the fluorophore moiety. In particular, during the MD simulation (visualization of run3 trajectory selected as example, Video S2) the sulfonic groups established salt bridges with K153 (persistent) and K150 (intermittent) in EL2, one of the amine moieties interacted with the sidechain of E169 (EL2), and the carboxylate moiety of the ligand replaced E169 (EL2) in the salt bridge with H264 (EL3). Moreover, for most of the total simulated time, the pyrazolotriazolopyrimidine core maintained its interaction pattern with N253 (6.55) and F168 (EL2), while the linker between the core and the fluorophore group was anchored to TM7, EL2 and TM2 through H-bond interactions with the backbone of S67 (2.65) and the sidechains of Q157 (EL2) and Y271 (7.36), respectively (Video S2).

Thus, both **11** and **12** are bitopic in the sense that each bridged two separate domains of the $A_{2A}AR$, i.e. the orthosteric binding site that is well defined in X-ray structures^{16,17} and an additional domain. The BODIPY630/650 fluorophore of **11** is predicted to be buried in a hydrophobic region, while

AlexFluor488 of **12** associates with the hydrophilic ELs. The bitopic nature of these conjugates does not necessarily imply allosteric modulation of the orthosteric action,²⁸ which is unexplored in this series.

In order to further explore ligand interaction with the EC surface, we prepared an aryl sulfonate **13**, which contained a terminal group capable of multiple polar interactions (Scheme S1, Supporting Information). This terminal phenylsulfonic acid moiety also would allow for π - π interactions with aromatic residues. A further benefit of incorporating a sulfonate group is that it carries a permanent negative charge at physiological pH and would prevent penetration of the blood brain barrier,²² a useful characteristic in a pharmacological probe for in vivo studies.²⁴ **13** was potent and selective in binding to the h and mA_{2A}ARs, with selectivity compared to the hA₁AR and hA₃AR of 671- and 426-fold, respectively. **13** binding to the mA₁AR and mA₃AR was insignificant.

The binding of **13** was modeled using the same docking procedure and MD validation described for **6c**. Figure 3 depicts the three alternative binding modes of **13**. In the most energetically favorable pose (BM1, blue carbon sticks) the sulfophenyl ring established a π - π stacking interaction with H264 (EL3) and the sulfonic group engaged in an H-bond interaction with the residue backbone. In the other two docking poses (BM2 and BM3, magenta and orange carbon sticks, respectively) the sulfophenyl ring established a π -cation interaction with K153 (EL2) and the sulfonic group interacted with the side chain of either K153 (EL2; BM2, magenta) or S156 (EL2; BM3, orange). During the MD simulation, the ligand's sulfophenyl tail fluctuated considerably (high averaged Root Mean Square Deviation values, Table S1), thus demonstrating the instability of the interaction pattern predicted in the initial docking poses. On the other hand, the three different initial poses converged in a unique binding mode, as the ligand-protein complexes with the lowest IE value returned by each different binding mode featured the

same conformation (Figure S5). In particular, the 7-phenylpropyl ring moved toward TM7 to establish a π - π stacking interaction with Y271 (7.36).

Two representative derivatives were shown to be A_{2A} AR antagonists in a cyclic AMP assay (Figure S6). The activation curve for known agonist **15** was right-shifted in a parallel manner by fixed concentrations of **11** and **13**. The EC_{50} of **15** was shifted from 0.89 ± 0.17 nM to 128 ± 35 nM in the presence of **11** (1000 nM) and to 10.2 ± 2.3 nM in the presence of **13** (100 nM). Off-target binding activities at 45 diverse receptors were determined by the PDSP²⁵ for selected compounds: **6c** and **13** (Supporting information). The only K_i values below 10 μ M were: **6c**, 3.36 μ M, 5HT_{2A} serotonin receptor; 1.92 μ M, 5HT_{2B} receptor. Thus, the primary amine precursor of the fluorescent conjugates **10** - **12** was not promiscuous in its interaction with other proteins, i.e. this chemical series is not associated with pan-assay interference compounds.²⁶

Compounds **11** and **12** were tested as fluorescent tracers for flow cytometry of HEK-293 cells expressing the hA_{2A}AR (Figure 4A). **11** proved to have high nonspecific binding, with a low level of specific binding amounting to <25% of total and therefore was not optimal for flow cytometric analysis. Thus, **11** tended to bind non-specifically to hydrophobic membranes by undetermined mechanisms. However, the more hydrophilic **12** displayed low nonspecific binding by this method, and its binding was saturable with a K_d value of 45.4 nM (Figure 4B). For inhibition studies, the cells were co-incubated for one hour prior to flow cytometry with fluorescent probe **12** (10 nM) and a test antagonist. Binding of **12** was inhibited by two known A_{2A}AR antagonists, nonxanthine **3** and xanthine **17**, with the expected range of potency. The K_i values were 3.8 and 17.2 nM (Figure 5), respectively, which corresponded

closely to the reported values of 4.1 and 18 nM at hA_{2A}AR.^{1,13} Agonist inhibition of competitive binding of **12** was complex (Supporting information).

Conclusions

We succeeded in identifying useful A_{2A}AR probes by systematically varying the chain length of amine-functionalized congeners of a potent antagonist and coupling the primary amine having an optimal length to various fluorophores. We successfully enhanced the A_{2A}AR affinity compared to known fluorescent A_{2A}AR ligands.¹⁵ Conjugates **11** and **12** were potent and selective antagonist probes for the A_{2A}AR, but **12** was more promising for characterization of the hA_{2A}AR in whole cells by flow cytometry. Molecular modeling suggested that the fluorophores of **11** and **12** interacted with the A_{2A}AR at distinct locations separate from the orthosteric binding site. The BODIPY630/650 moiety of **11** was predicted to associate with hydrophobic regions between TMs. However, the hydrophilic fluorophore of **12** was coordinated to the ELs, consistent with its lower overall hydrophobicity and more favorable whole cell binding characteristics compared to **11** under present conditions. An evaluation of **11** and **12** in confocal microscopy studies remains to be performed. Thus, we have introduced antagonist ligands displaying high A_{2A}AR affinity and selectivity that may serve as versatile tools to better study this receptor.

Acknowledgements

This research was supported in part by the Intramural Research Program of the NIH, National Institute of Diabetes and Digestive and Kidney Diseases. RD was supported by Inserm, Univ. Lille, France. We

thank Dr. John Lloyd (NIDDK) for mass spectra. SB was supported by UGC, India. JA acknowledges support from National Heart, Lung, and Blood Institute (R01HL133589).

Supporting information

Supplementary data (5 files) can be found, in the online version, at doi:xxxxxxx.

- 1) chemical synthesis, characterization data, HPLC analysis, pharmacological studies, off-target screening and additional molecular modeling procedures/results.
- 2) 3D coordinates of the hA_{2A}AR in complex with **11** (docking pose).
- 3) 3D coordinates of hA_{2A}AR in complex with **12** (docking pose, BM2).
- 4) Video of 30 ns of MD simulations of hA_{2A}AR in complex with **3**. **Video S1**. Trajectory visualization (left panel) and ligand-protein interaction energy profile (right panel) of 30 ns of membrane MD simulation of the **3**-hA_{2A}AR complex.
- 5) Video of 30 ns of MD simulations of hA_{2A}AR in complex with **12**. **Video S2**. Trajectory visualization of 30 ns of membrane MD simulation of the **12**-hA_{2A}AR complex starting from docking binding mode denoted as "BM2": side view facing TM5, TM6, and TM7 (left panel), and side view facing TM4, TM5 and TM6 (right panel).

Conflict of interest

The authors declare no competing interests.

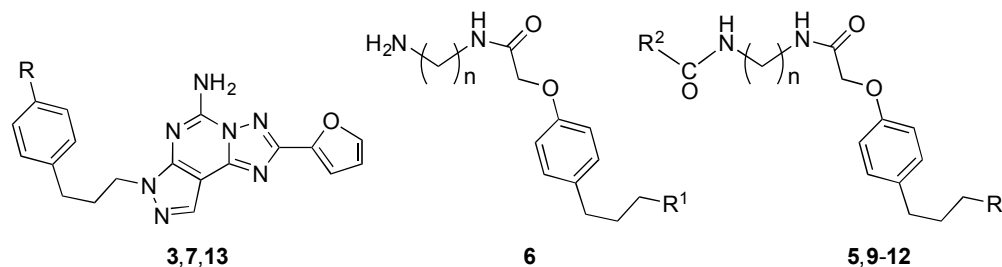
References and Notes

1. C. E. Müller and K. A. Jacobson, *Biochim. Biophys. Acta - Biomembranes*, 2011, **1808**, 1290-1308.
2. G. Yuan, N. G. Gedeon, T. C. Jankins, and G. B. Jones, *Expert Opinion on Drug Discovery*, 2015, **10**, 63-80.
3. P. G. Baraldi, M. A. Tabrizi, S. Gessi, and P. A. Borea, *Chem. Rev.* 2008, **108**, 238-263.
4. C. V. Gomes, M. P. Kaster, A. R. Tomé, P. M. Agostinho and R. A. Cunha, *Biochim. Biophys. Acta - Biomembranes*, 2011, **1808**, 1380-1399.

5. C. Laurent, S. Burnouf, B. Ferry, V. L. Batalha, J. E. Coelho, Y. Baqi, E. Malik, E. Mariciniak, S. Parrot, A. Van der Jeugd, E. Faivre, V. Flaten, C. Ledent, R. D'Hooge, N. Sergeant, M. Hamdane, S. Humez, C. E. Müller, L. V. Lopes, L. Buée and D. Blum, *Molecular Psychiatry*, 2016, **21**, 97-107.
6. S. M. Hatfield and M. Sitkovsky, *Curr. Opin. Pharmacol.* 2016, **29**, 90-96.
7. P. A. Beavis, M. A. Henderson, L. Giuffrida, J. K. Mills, K. Sek, R. S. Cross, A. J. Davenport, L. B. John, S. Mardiana, C. Y. Slaney, R. W. Johnstone, J. A. Trapani, J. Stagg, S. Loi, L. Kats, D. Gyorki, M. H. Kershaw and P. K. Darcy, *J. Clin. Invest.* 2017, doi:10.1172/JCI89455
8. M. T. Armentero, A. Pinna, S. Ferré, J. L. Lanciego, C. E. Müller and R. Franco, *Pharmacol. Therap.* 2011, **132**, 280-299.
9. M. H. Madeira, R. Boia, A. F. Ambrósio and A. R. Santiago, *Mediators of Inflammation*, vol. 2017, Article ID 4761081, 12 pages, 2017. doi:10.1155/2017/4761081
10. T. Kondo, Y. Mizuno, *Clin. Neuropharm.* 2015, **38**, 41-46.
11. A. F. Ramlackhansingh, S. K. Bose, I. Ahmed, F. E. Turkheimer, N. Pavese and D. J. Brooks, *Neurology* 2011, **76**, 1811-1816.
12. X. Zhou, S. Khanapur, A. P. Huizing, R. Zijlma, M. Schepers, R. A. J. O. Dierckx, A. van Waarde, E. F. J. de Vries and P. H. Elsinga, *J. Med. Chem.* 2014, **57**, 9204-9210.
13. T. S. Kumar, S. Mishra, F. Deflorian, L. S. Yoo, K. Phan, M. Kecskés, A. Szabo, B. A. Shinkre, Z. G. Gao, W. C. Trenkle and K.A. Jacobson, *Bioorg. Med. Chem. Lett.* 2011, **21**, 2740-2745.
14. Kecskés, M.; Kumar, T. S.; Yoo, L.; Gao, Z. G. and Jacobson, K. A. *Biochem. Pharmacol.* 2010, **80**, 506-511.
15. F. Ciruela, V. Fernández-Dueñas and K.A. Jacobson, *Neuropharmacology* 2015, **98**, 58-67.
16. V. P. Jaakola, M. T. Griffith, M. A. Hanson, V. Cherezov, E. Y. T. Chien, J. R. Lane, A. P. IJzerman, and R. C. Stevens, *Science* 2008, **322**, 1211.
17. W. Liu, E. Chun, A. A. Thompson, P. Chubukov, F. Xu, V. Katritch, G. W. Han, C. B. Roth, L. H. Heitman, A. P. IJzerman, V. Cherezov and R. C. Stevens *Science* 2012, **337**, 232-236.
18. C. J. Langmead, S. P. Andrews, M. Congreve, J. C. Errey, E. Hurrell, F. H. Marshall, J. S. Mason, C. M. Richardson, N. Robertson, A. Zhukov and M. Weir *J. Med. Chem.* 2012, **55**, 1904-1909.
19. V. Katritch, V. P. Jaakola, J. R. Lane, J. Lin, A. P. IJzerman, M. Yeager, I. Kufareva, R. C. Stevens and R. Abagyan, *J. Med. Chem.* 2010, **53**, 1799.
20. D. Rodriguez, Z.G. Gao, S.M. Moss, K.A. Jacobson and J. Carlsson, *J. Chem. Inf. Model.* 2015, **55**, 550-563.
21. L. D. Lavis and R. T. Raines, *ACS Chem. Biol.* 2008, **3**, 142-155.
22. S. Paoletta, D. K. Tosh, A. Finley, E. Gizewski, S. M. Moss, Z. G. Gao, J. A. Auchampach, D. Salvemini and K. A. Jacobson, *J. Med. Chem.* 2013, **56**, 5949-5963.
23. J. A. Ballesteros and H. Weinstein, *Methods Neurosci.* 1995, **25**, 366.
24. J. L. Carlin, D. K. Tosh, C. Xiao, R. A. Piñol, Z. Chen, D. Salvemini, O. Gavrilova, K. A. Jacobson and M. L. Reitman, *J. Pharmacol. Exp. Therap.* 2016, **356**, 474-482.
25. J. Besnard, G. F. Ruda, V. Setola, K. Abecassis, R. M. Rodriguiz, X. P. Huang, S. Norval, M. F. Sassano, A. I. Shin, L. A. Webster, F. R. Simeons, L. Stojanovski, A. Prat, N. G. Seidah, D. B. Constam, G. R. Bickerton, K. D. Read, W. C. Wetsel, I. H. Gilbert, B. L. Roth and A. L. Hopkins, *Nature* 2012, **492**, 215-220.
26. C. Aldrich, C. Bertozzi, G. I. Georg, L. Kiessling, C. Lindsley, D. Liotta, K. M. Merz, Jr., A. Schepartz and S. Wang. *ACS Chem. Biol.* 2017, **12**, 575-578.
27. C. E. Müller and K. A. Jacobson, Xanthines as adenosine receptor antagonists. In Methylxanthines, B.B. Fredholm, ed., Springer, *Handb. Exp. Pharmacol.* 2011, 200:151-199.

28. G. Vauquelin, D. Hall and S. J. Charlton, *Br. J. Pharmacol.* 2015, **172**, 2300–2315.

Table 1. AR binding affinity determined for a series of pyrazolo[4,3-*e*][1,2,4]triazolo[1,5-*c*]pyrimidin-5-amine derivatives (R^1 , as in Scheme 1). Human ARs, unless noted (m indicates mouse).



Compd	Structure	Affinity, K_i , nM (or %inhib)		
		A_1^a	A_{2A}^a	A_3^a
3^b	R = OCH ₃	(35±5%) ^c	4.1 ^e	(67±1%) ^c
5^b	R ² = AlexaFluor488 ^d , n = 2	(20±3%) ^c	111±16 ^c	(4±2%) ^c
6a^b	n = 2	1270±140 ^c	6.8±1.1 ^e	3970±120
6b	n = 3	1300±350	9.29±7.92	2170±660
6c	n = 4	2390±100	6.46±1.63	5990±2900
6d	n = 5	1910±120	6.36±3.58	656±132
6e	n = 6	6500±2830	22.8±8.45	2070±850
7^b	R = -OH	(66±2%) ^c	48±28 ^e	(34±3%) ^c
9	R ² = AlexaFluor647 ^d , n = 2	(13±6%) ^c , (3±1%) ^c (m)	332±165, 458±24 (m)	(21±3%) ^c , (4±1%) ^c (m)
10	R ² = AlexaFluor647 ^d , n = 4	(20±3%) ^c	295±176	(21±2%) ^c
11^f	R ² = BODIPY630/650 ^d , n = 4	(40±3%) ^c , (0%) ^c (m)	24.6±17.6, 2.09±0.16 (m)	(33±5%) ^c , (2±2%) ^c (m)
12^f	R = AlexaFluor488 ^d , n = 4	1680±470, (0%) ^c (m)	30.3±4.9, 585±73 (m)	(32±3%) ^c , (5±2%) ^c (m)
13^f	R = -OCH ₂ -Ph- <i>p</i> -SO ₃ H	4190±750, (21±4%) ^c (m)	6.24±2.42, 64.1±5.3 (m)	2660±1250, (4±1%) ^c (m)

a. Competition radioligand binding assays were conducted with membranes prepared from HEK-293 cells expressing recombinant A_1 , A_{2A} , or A_3 AR, human, unless noted. Incubations were performed for 1 h at 25 °C. The radioligands used were: A_1 AR, [³H]8-cyclopentyl-1,3-dipropylxanthine ([³H]DPCPX, 0.5 nM)

14; A_{2A}AR, [³H]ZM241385 **2** (1.0 nM) or if from published data¹³ (as noted) [³H]2-[p-(2-carboxyethyl)phenyl-ethylamino]-5'-N-ethylcarboxamidoadenosine ([³H]CGS21680, 10 nM) **15**; A₃AR, [¹²⁵I]N⁶-(4-amino-3-iodobenzyl)adenosine-5'-N-methyluronamide ([¹²⁵I]I-AB-MECA, 0.2 nM) **16**. Nonspecific binding was determined using 10 μM 8-[4-[[[(2-aminoethyl)amino]carbonyl]methyl]oxy]phenyl]-1,3-dipropylxanthine (XAC) **17** (A₁AR and A_{2A}AR) or 10 μM adenosine-5'-N-ethyluronamide (NECA) **18** (A₃AR). HEK-293 cells expressing recombinant mA₁, mA_{2A}, or mA₃AR were used. Values are expressed as the mean ± SEM from 3 independent experiments. The cell lines were from American Type Culture Collection (ATCC, Manassas, VA), and the cDNA for the ARs was obtained from cdna.org.

- b. Data from Kumar et al. and Kecskés et al.^{13,14}
- c. Percent inhibition at 10 μM.
- d. Fluorophore moiety, as shown in Scheme 1 (R²).
- e. Using [³H]**16** as radioligand.
- f. **11**, MRS7396; **12**, MRS7416; **13**, MRS7352.

Figures and Legends

Figure 1. Antagonist radioligand ($[^3\text{H}]2$, 1.0 nM) binding inhibition curves at the $\text{hA}_{2\text{A}}\text{AR}$ for four antagonist fluorescent conjugates. Compound numbers: MRS7322 **9**, MRS7395 **10**, MRS7396 **11**, MRS7416 **12**. Membranes from HEK-293 cells expressing the $\text{hA}_{2\text{A}}\text{AR}$ were used, and incubations were performed for 1 h at 25 °C. Results are expressed as the mean \pm SEM. The K_i values from three independent experiments are listed in Table 1.

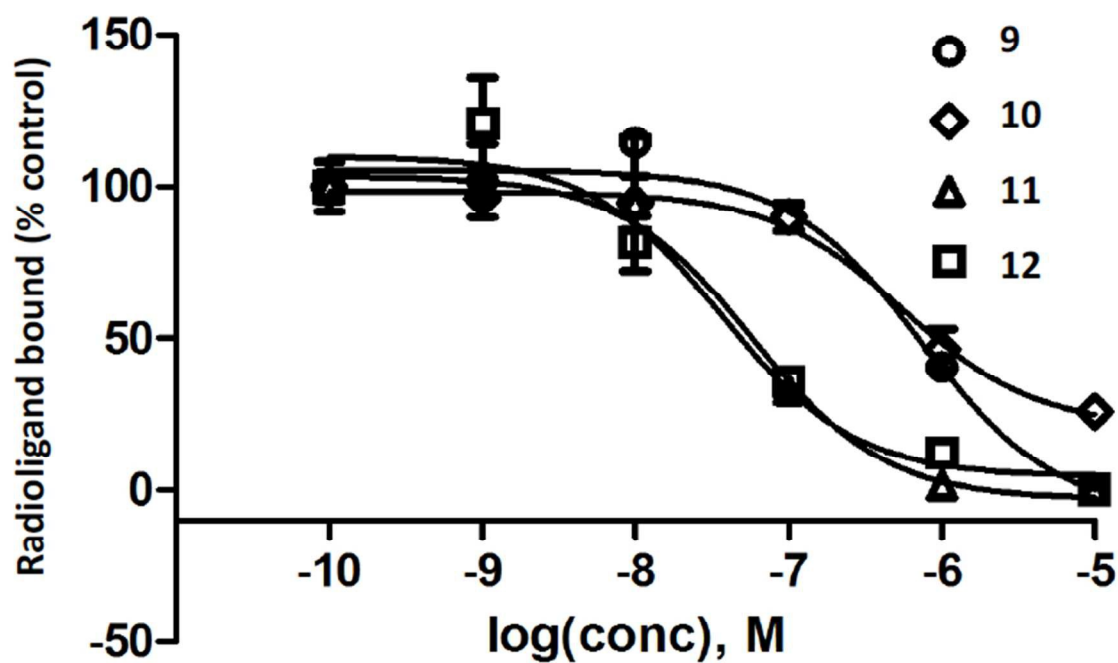


Figure 2. Molecular modeling of antagonist binding to the hA_{2A}AR. Details of the binding site of the X-ray structure of the receptor modeled with various ligands docked: (A) known antagonist **3**, with the retention of a subset of water molecules found in the high resolution A_{2A}AR structure¹⁷; (B) the BODIPY630/650-labeled antagonist **11**, showing the most energetically favorable orientation of the terminal fluorophore chain; side (C) and top (D) view of the two possible orientations of the fluorophore group of derivative **12**. Residues establishing polar (dashed orange lines) and π - π interactions with the docked ligands are represented as sticks. Aromatic residues establishing hydrophobic contacts with the terminal fluorophore of compound **11** are represented as transparent surfaces with colors matching the corresponding TM domain. Non-polar hydrogen atoms are omitted.

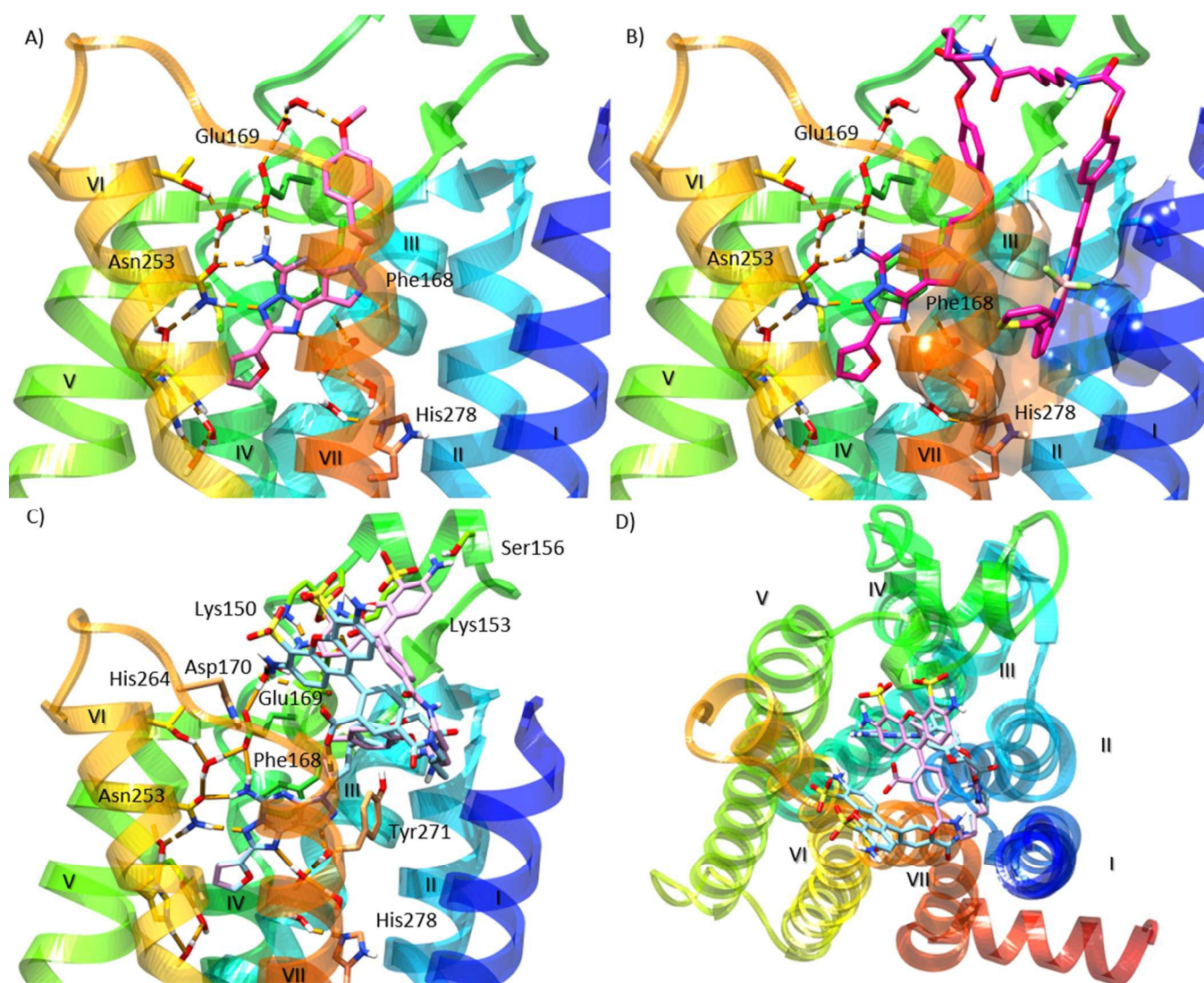


Figure 3. Modeling of antagonist **13** binding to the hA_{2A}AR: side (C) and top (D) view of the three possible orientations (BM1, blue; BM2, magenta; BM3, orange) of the *p*-sulfophenyl tail. Residues establishing polar (dashed orange lines) and π - π interactions with the docked ligands are represented as sticks. Non-polar hydrogen atoms are omitted.

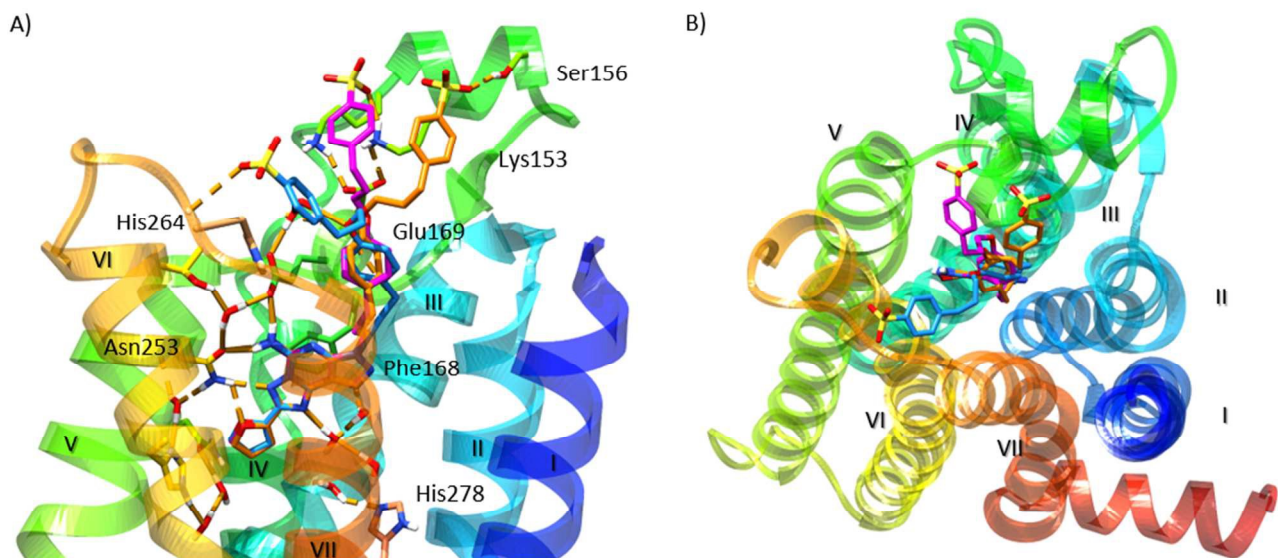


Figure 4. Saturation of fluorescent antagonists **11** (A) and **12** (B) in hA_{2A}AR-expressing HEK-293 cells measured using flow cytometry following a 1 h incubation at 37 °C. Non-specific binding was determined with 10 μM **3**. Results are expressed as the mean ± SEM. The K_d value calculated from from Figure 4B is listed in the text.

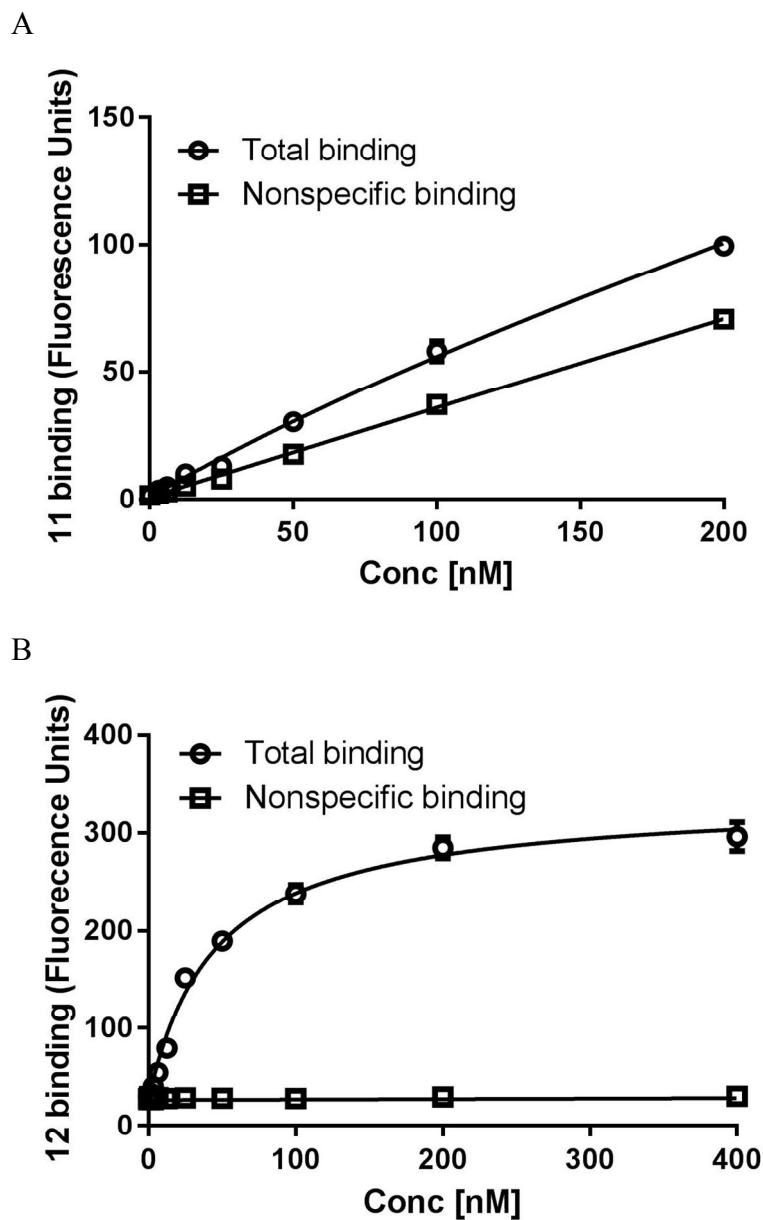


Figure 5. Inhibition of the specific binding of fluorescent antagonist **12** (10 nM, 1 h incubation at 37 °C) in hA_{2A}AR-expressing HEK-293 cells measured using flow cytometry. Competing antagonists were: nonxanthine **3** and xanthine **17**. Non-specific binding was determined with 10 μM **3**. Results are expressed as the mean ± SEM. The K_i values are listed in the text.

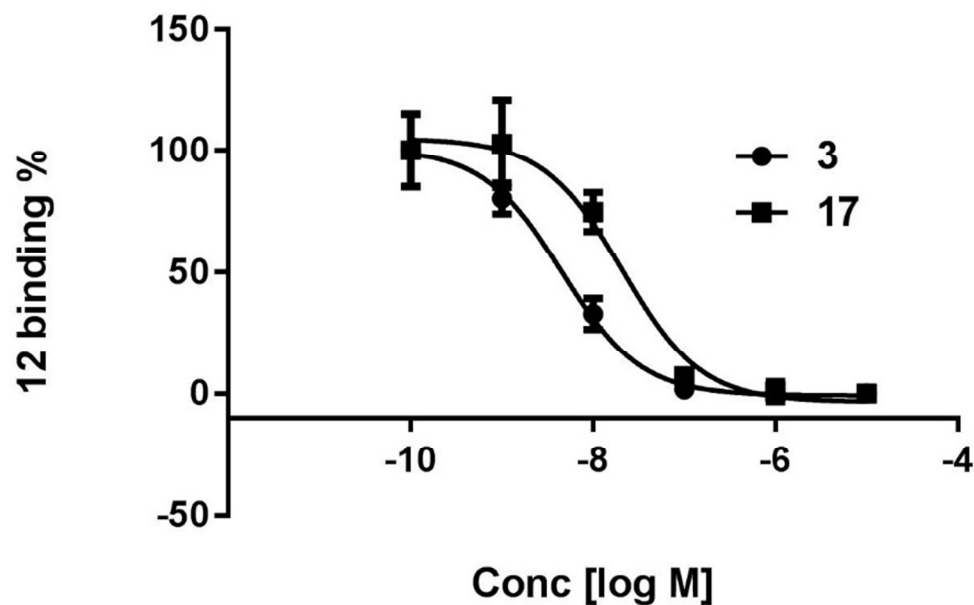


Table of contents entry

Bitopic Fluorescent Antagonists of the A_{2A} Adenosine Receptor Based on Pyrazolo[4,3-e][1,2,4]triazolo[1,5-c]pyrimidin-5-amine Functionalized Congeners

Romain Duroux, Antonella Ciancetta, Philip Mannes, Jinha Yu, Shireesha Boyapati, Elizabeth Gizewski, Said Yous, Francisco Ciruela, John A. Auchampach, Zhan-Guo Gao, and Kenneth A. Jacobson

